気象研究所研究報告　第54巻第2号　71－90頁　平成15年12月
Papers in Meteorology and Geophysics Vol. 54, No. 2, pp. 71－90, December 2003

GRIPS Solar Experiments Intercomparison Project: Initial Results

By

K. Matthes,
Institut für Meteorologie, Freie Universität Berlin, Germany

K. Kodera,
Meteorological Research Institute, Tsukuba, Japan

J. D. Haigh,
Imperial College of Science, Technology and Medicine, London, UK

D. T. Shindell,
NASA Goddard Institute for Space Studies and Center for Climate Systems Research, Columbia University, New York, USA

K. Shibata,
Meteorological Research Institute, Tsukuba, Japan

U. Langematz,
Institut für Meteorologie, Freie Universität Berlin, Germany

E. Rozanov,
University of Illinois, Urbana-Champaign, USA; now: PMOD/WRC and IAC ETH, Davos, Switzerland

and

Y. Kuroda
Meteorological Research Institute, Tsukuba, Japan

(Received October 31, 2002 ; Revised March 28, 2003)

Abstract

The GRIPS solar intercomparison project presented here is part of the "GCM Reality Intercomparison Project for SPARC (GRIPS)" focusing only on the influence of 11-year solar-cycle variations on the atmosphere. The aim of the present comparison is to assess the problems related to the simulation of the solar influence in order to better define future experiments. Results from different GCMs will be presented to investigate whether there is any consistency between them or with existing model studies and observations. Each of the different GCMs used the same wavelength-dependent solar irradiance changes as well as the resulting ozone changes calculated with 2-D chemical models enabling a better intercomparison of the different GCMs. It turns out that each model response is different and that the model results are dependent on the model climatologies that vary widely both among themselves and with observations.

One of the major problems encountered during the comparison is the lack of reliable observational evidence for the solar influence on climate (e.g., temperature, ozone). There are also important uncertainties of the forcings used for the model simulations (solar energy spectrum, ozone).

1. Introduction

General Circulation Model (GCM) studies are important for better understanding climate change and variability, which can be of natural origin (e.g., sun, Quasi-Biennial Oscillation (QBO), El Nino Southern Oscillation (ENSO), volcanoes) or anthropogenic origin (greenhouse gases (GHG), chlorofluorocarbons (CFCs)). The use of GCMs permits quantitative

Corresponding author: Katja Matthes, matthes@strat01.met.fu-berlin.de

estimates of individual factors. The present GCM study is part of the "GCM Reality Intercomparison Project for SPARC" (GRIPS) (Pawson et al., 2000) and will focus on the impact of the 11-year solar cycle as an external, natural climate factor on the atmospheric circulation. Estimates of the total solar irradiance (e.g. Lean et al., 1997) show small changes of the solar "constant" (~0.1%) between the maximum and minimum of 11-year solar variations integrated over the solar spectrum. In the ultraviolet (UV) range of the solar spectrum however, which is important for ozone production and loss, irradiance variations can reach up to 8% near 200nm (Fig. 1).

Statistical investigations with observational data have revealed high correlations between meteorological parameters in the lower stratosphere, e.g., temperature and geopotential height, and the 11-year solar cycle (Labitzke, 1987; Labitzke and van Loon, 1988; Labitzke, 2001). The impact of solar irradiance changes on the tropospheric circulation, e.g., a change in the Hadley circulation, has also been investigated in observational and modelling studies (Labitzke and van Loon, 1999; Haigh, 1999). However, a complete mechanism for the influence of solar irradiance changes on atmospheric circulation is still missing.

The first modelling studies using realistic solar irradiance data and estimated ozone changes (Haigh, 1996; Shindell et al., 1999) discussed the possibility of an indirect dynamical response of the lower atmosphere to the radiative forcing of the upper atmosphere. Depending on the time of year (Fig. 2a) enhanced UV radiation during solar maxima leads to enhanced ozone production in the upper stratosphere (maximal 3% near 5 hPa from the subtropics to higher latitudes). During solar maxima, the enhanced UV radiation as well as the enhanced ozone lead to a greater shortwave heating rate in the stratosphere than during solar minima. The thermal gradient induced directly in the upper stratosphere (near the stratopause at a height of 50 km) can alter the mean meridional circulation from the stratosphere down to the troposphere by affecting the planetary wave propagation in the winter hemisphere.

Kodera (1991) pointed out that the sun as well as the QBO produces wind anomalies in the upper subtropical stratosphere in early winter (December). Such wind anomalies change the propagation properties for planetary waves and affect the polar night jet formation at higher latitudes through wave-mean flow interactions and also affect the Brewer-Dobson circulation. Via this positive feedback mechanism, the wind anomalies propagate poleward and downward during wintertime from the upper stratosphere at lower latitudes to the lower stratosphere at higher latitudes. Kodera (1991, 1995) confirmed the observed modulation between solar and QBO signals (Labitzke and van Loon, 1988) during winter and assumed that the solar activity as well as the QBO (and volcanic eruptions) trigger the interannual variability of the stratosphere. New studies indicate that during early winter the stratosphere is mainly in a radiatively controlled state, which is characterised by strong zonal winds and weak wave forcing. Later in winter, the stratospheric circulation then switches from a radiatively controlled to a dynamically controlled state (Kodera and Kuroda, 2002). During solar maximum years the radiatively controlled state seems to last longer.

In order to study the magnitude of the solar impact, coordinated experiments using the same forcing are performed under the GRIPS initiative. As a first step, new GCM experiments using identical ozone and solar irradiance changes are compared with similar existing model studies (Haigh, 1999; Shindell et al., 1999, Larkin et al., 2000; Shindell et al., 2001) to examine if the results are model-dependent.

We concentrate on the influence of solar UV heating rate changes because changes in this part of the solar spectrum show the largest variability in observations, and model results indicate a great impact of the UV variability on the atmosphere. The stratosphere is warmed through the absorption of UV light while the Earth's surface (mainly ocean) is warmed through the absorption of visible light. However, the latter mechanism is not taken into account in the GCM studies presented here because seasonally varying climatological sea surface temperatures (SSTs) were used for efficiency reasons. This enabled integrating the models for 20 years under perpetual solar conditions focusing on the impact of solar UV variations, which have the largest impact in the stratopause region.

One of the major problems is the lack of reliable observational evidence for the solar influence on climate (e.g., temperature, ozone). There are also important uncertainties of the forcings used for the model simulations (solar energy spectrum, ozone). This study summarizes the results of solar experiments from four different GCMs participating in the GRIPS initiative; in the discussion a fifth GCM with interactive chemistry is shown for comparison. The aim of the present comparison is to assess the problems related to the simulation of the solar influence to better define future experiments.

This paper is structured as follows: Section 2 describes the experimental design with solar irradiance and ozone changes and the participating GCMs.

Section 3 shows the results of the different model studies. Section 4 discusses the different model studies. Section 5 presents the conclusion.

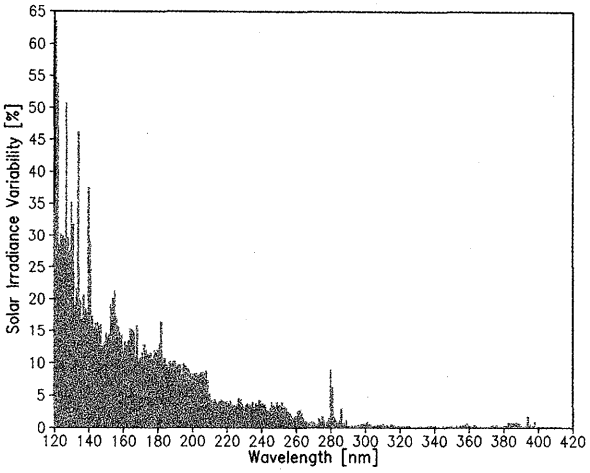

Fig. 1: Estimated solar irradiance changes in the UV part of the spectrum from 120-420 nm during the 11-year solar cycle in percent, data from Lean et al. (1997).

2. Experimental Design

To simulate the 11-year solar cycle in GCM experiments, the spectral solar irradiance changes between solar maximum and minimum as well as resulting ozone differences calculated with two different chemical models have been implemented in the GCMs. Each of the GCMs used the same prescribed changes for solar irradiance data. However, only one GCM performed experiments with both available ozone change fields while the other models used only one of the available ozone change fields. The implemented changes described in the following enabled a better intercomparison of different GCMs (which use the same irradiance and ozone changes and of those using the same irradiance but different ozone change fields), and an investigation of the importance of the used ozone change fields (GCM experiments using both ozone change fields in the same model).

Groups and GCMs participating in the GRIPS solar intercomparison project are briefly summarized in Table 1. For further details concerning model characteristics etc., see the GRIPS report (Pawson et al., 2000).

2.1 Solar Energy Spectrum

The solar irradiance data from 119.5 to 419.5 nm (spectral resolution of 1 nm) used here are estimated with a multiple-regression model using a UV sunspot darkening index and the Mg facular proxy index (Lean et al., 1997). The estimated solar cycle variations used for the GCM experiments are based on satellite observations from November 1989 for solar-maximum conditions and from September 1986 for solar-minimum conditions. Figure 1 shows the percentage change of solar irradiance variations between solar maximum and minimum at wavelength intervals from 120 to 420nm. The GISS model used solar irradiance changes from 120 to 400nm, and constant changes at longer wavelengths consistent with total solar cycle irradiance variations; the IC model included changes in the solar spectrum throughout the near-infrared and visible. The three other models (MRI, FUB, UIUC) used the solar irradiance changes only for the UV part of the spectrum longer than about 200nm. The solar irradiance changes were integrated over the individual spectral bands in the (shortwave) radiation schemes of each GCM (see Table 2 for details).

2.2 Ozone Variation

The percentage ozone differences between solar maximum and solar minimum years were calculated off-line with two different models. One was a two-dimensional (2-D) photochemical-transport model (Haigh, 1994); ozone variations from this model will be marked with "IC" in the following text. The other employed an interactive chemical parameterisation of the GISS GCM (Shindell et al., 1999). Ozone variations from this model will be marked with "GISS". The GISS chemistry parameterisation included a wavelength-dependent ozone response to changes in radiation and temperature. Ozone was not transported in the model. Whereas the IC ozone showed two maxima of 3% more ozone during solar maxima in the annual mean around 30°-60° S and 30-60° N between 10 and 5 hPa (Fig. 2a), the GISS ozone field (Fig. 2b) showed only one maximum of 2.5% around the equator between 3 and 5 hPa, at a slightly higher altitude than the maxima in the IC ozone field. For the GISS ozone above 5 hPa the larger variation due to the temperature feedback of the ozone field can be clearly seen at higher northern and southern latitudes indicating a response to dynamical heating.

Two GCM' s used the GISS ozone (GISS and MRI-G), whereas three GCM' s used the IC ozone (IC, MRI-I, FUB) as shown in Table 2. The MRI model was the only GCM, which performed the solar experiments twice (with GISS and IC ozone). Therefore the effect of the ozone distribution can be studied additionally with these experiments.

Table 1: List of the groups and GCMs participating in the GRIPS solar intercomparison project.

Group	Model	Horizontal Resolution	Top Level	Vertical Layers	GW Drag	Reference
GISS	GISS LR grid model	8°x10°	0.002 hPa	23	orographic, convective, shear instabilities	Rind et al., 1988a,b
IC	UK Met.Office Unified Model	2.5°x3.75°	0.1 hPa	58	orographic (p>20 hPa), MRF*	Swinbank et al., 1998
MRI	MRI/JMA98	T42 (2.8°x2.8°)	0.01 hPa	45	MRF	Shibata et al., 1999
FUB	FUB-CMAM	T21 (5.6°x5.6°)	0.0068 hPa	34	MRF	Langematz and Pawson, 1997; Pawson et al., 1998; Langematz, 2000
UIUC	UIUC 24L ST-GCM/PC	4°x5°	1 hPa	24	orographic	Rozanov et al., 2001

*MRF: mesospheric Rayleigh friction

Table 2: List of SW radiation schemes in the GCMs (see also radiation intercomparison project for GRIPS, Langematz et al., in preparation), number of spectral intervals in the SW part where solar irradiance changes have been implemented, reference ozone field, and ozone changes due to solar irradiance changes calculated with 2D chemical models (which use different radiation codes from the GCMs).

Group	SW radiation code	Number of changed SW spectral intervals	Reference ozone climatology	Solar induced ozone changes
GISS	Hansen et al. (1983)	analytic absorp. function 115-900 nm in 5 to 10 nm steps for O_3, 300-900 nm: 6 bands for other gases	LIMS satellite data; parameterized ozone	GISS
IC	Edwards and Slingo (1996)	200-23800nm: 6	Keating et al. (1987) (p<22.5mb); SBUV (McPeters p.c.) elsewhere	IC
MRI	Briegleb (1992), Shibata and Uchiyama (1994)	200-350nm: 7 350-700nm: 1	Wang et al. (1995) (p>0.28 hPa); Keating et al. (1987) (p<0.28 hPa)	GISS, IC (MRI-G), (MRI-I)
FUB	Fouquart and Bonnel (1980); modified Shine and Rickaby (1989); Strobel, (1978)	206.2-852.5nm: 44	Update of Fortuin and Langematz (1994)	IC
UIUC	Chou (1990,1992); Chou and Lee (1996); Chou and Suarez (1999)	175-700nm: 8	Interactively calculated	—

2.3 GCM integrations

For each model two twenty year runs, have been performed, both in an annual cycle mode. One representing "perpetual" solar minimum the other one representing "perpetual" solar maximum conditions. The internal variability in the stratosphere of each GCM is largely due to the irregular occurrence of stratospheric warmings (see, e.g., Pawson et al., 2000, their Fig. 6); therefore it was necessary to simulate sufficient model years. Since the solar forcing was not changed with a realistic 11-year solar irradiance periodicity, these idealised model experiments allowed a statistical analysis for 20 year solar maximum and 20 year solar minimum. The economy of calculation time was another important reason for the performance of the experiments in this way; integrating a realistic 11-year solar cycle would need model runs of 100 years or so to get statistically significant results. Such experiments are beyond the currently available computer time.

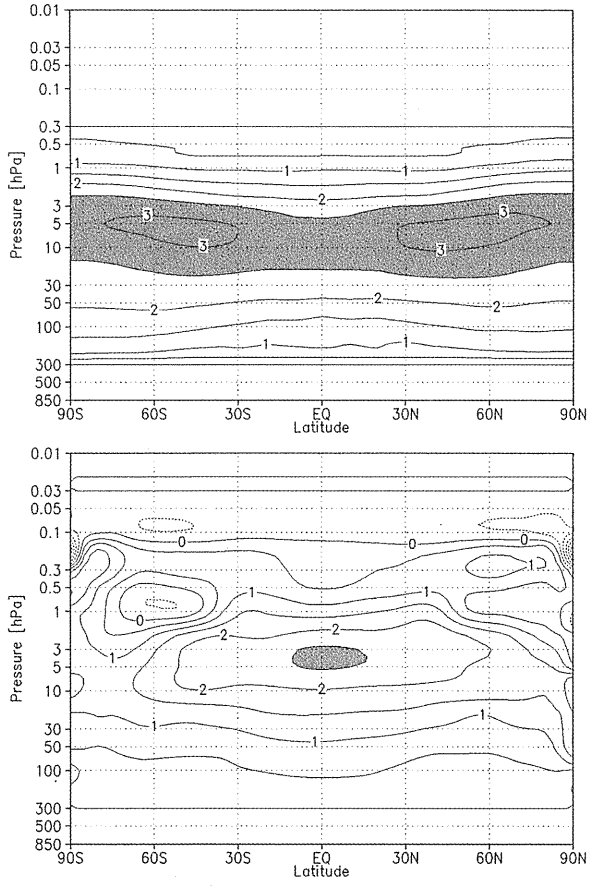

Fig. 2: Difference in the annual mean ozone between solar maximum and minimum in percent calculated with a) the 2-D chemical transport model from the Imperial College of Science, Technology and Medicine (Haigh, 1994) and b) the interactive chemistry parameterisation of the GISS GCM (Shindell et al., 1999); contour interval: 0.5%, values greater than 2.5% shaded for emphasis.

3. Results

One of the difficulties of investigating the solar response arises from its highly non-linear nature (Kodera and Kuroda, 2002). On the other hand, due to such non-linearity, a relatively small forcing could produce a large response. This means that the observed signal cannot simply be assumed to be "a sum of signal and uncorrelated noise". Thus, to understand the solar response, it should be analysed together with the interannual variation. Therefore, for the present report we have limited the discussion only to the illustration of the mean difference, leaving a more detailed analysis of the relationship between the mean differences and the interannual variations for a separate study (Kodera et al., 2003). Therefore, statistical significance based on the usual assumption is not plotted.

The following results are all based on differences between a long term monthly mean average of 20 solar maximum and 20 solar minimum years to characterize the long term mean impact of solar irradiance changes.

3.1 Shortwave Heating Rates

The difference between solar maximum and minimum in the annual mean shortwave heating rates (in Kelvin per day) is presented in Fig. 3 for the five experiments. Presented on the left-hand side are models that used the GISS ozone and on the right-hand side models that used the IC ozone. The difference in the shortwave heating rates shows the direct impact of solar irradiance and ozone changes. The largest response in all experiments appeared near the stratopause (~50 km height). However, the strength and the shape of the differences was model and ozone field dependent. Models in which the IC ozone was used showed a maximum difference in the tropical stratopause region. The MRI-I and the FUB model signals are of similar magnitude (0.21 K/day) whereas that of the IC model is much stronger (0.27 K/d). Those models using the GISS ozone showed two, rather distinct maxima in the shortwave heating rate differences near 20-30° North and South with a comparable magnitude as for the MRI-I and the FUB models (0.21 K/d). Note that the reasons for the reversed maximum structures in the SW heating rate differences (Fig.3) and in the ozone change fields (Fig.2) for GISS and IC will be investigated in a future study. At higher latitudes there were remarkable differences between the models, e.g., between the IC and the FUB model. The IC model showed a much larger difference (0.24 K/d) at southern high latitudes around 1 hPa than either the FUB or the MRI-I models (0.15 K/d). The differences could be caused by

differences in the radiation schemes or in the background ozone climatologies. Using a different ozone field in the same model, MRI-I and MRI-G, also gave slightly different results: the experiment with IC ozone reached 0.15 K/d whereas the experiment with GISS ozone reached 0.18 K/d in the southern high latitude stratopause region. This difference can be attributed to the differences in the ozone fields (IC and GISS) because the radiation scheme and the ozone climatology were not changed between these two experiments. It is also interesting to note that the IC SW heating rate differences are very high at SH latitudes (0.24 K/d) while the GISS SW heating rate differences are very low at the same latitude (0.12 K/d), only half of the IC difference. The MRI model produces a similar SW heating rate difference for both ozone change fields. So differences in the SW heating rate anomalies between MRI and IC/GISS can be attributed either to differences in the background ozone climatologies or differences in the radiation schemes.

3.2 Zonal Mean Temperature

In Fig. 4 the annual mean temperature difference between solar maximum and minimum for the five experiments is shown. The differences in temperature patterns in the stratopause region were very similar to the difference in the annual mean shortwave heating rates shown before (Fig. 3). A clear temperature signal (~1 K) appeared in each experiment in the tropical stratopause region which featured the higher shortwave heating rates (see Fig. 3). In every model the temperatures were higher during solar maxima than during solar minima throughout the tropical, subtropical and mid-latitude stratosphere and upper troposphere. The signal in higher northern and southern latitudes varied from model to model, probably due to different internal model variability. It was very different for the same model using different ozone fields (MRI-I and MRI-G). Here, the MRI-I experiment showed a negative anomaly northwards of 60° N for the troposphere up to the stratosphere, whereas the MRI-G experiment showed a dipole structure with positive anomalies lower down and slightly negative ones further up. The GISS, MRI-I, and FUB models showed the same structure at high northern latitudes with negative anomalies in the troposphere and stratosphere and positive anomalies above In the GISS model the positive anomalies reach farther down. The largest temperature signal appeared in the IC and the FUB models at lower latitudes whereas the maximum was shifted to high northern latitudes in the GISS model and the MRI-I experiment and to high southern latitudes in the MRI-G experiment. Except for the GISS and the FUB model, all models showed negative temperature anomalies at tropospheric southern mid and high latitudes. The FUB GCM was the only one having negative temperature anomalies in the tropical and subtropical lower mesosphere. The MRI and the GISS model showed a decrease of the temperature anomalies in the tropical and subtropical lower mesosphere, too, but less pronounced than in the FUB model. This difference is possibly due to the differences in the longwave radiation codes of the GCMs.

3.3 Zonal Mean Wind

The different zonal mean temperature structure (Fig. 4) between solar maximum and minimum is connected with differences in the zonal mean wind structure, as shown in Fig. 5 for the northern winter (November to February) and in Fig. 6 for the southern winter (June to September). The National Meteorological Centre (NMC) data are shown for comparison with the model data on the left column of Figs. 5 and 6, followed by models that used the GISS ozone and then by models that used the IC ozone. The zonal mean wind of the NMC data was derived from geopotential height data analysed from the National Centres for Environmental Prediction (NCEP), formerly the National Meteorological Centre (NMC) (Randel, 1992). Figures 5 and 6 show the differences between six solar maximum years (1980-1982 and 1989-1991) and ten solar minimum years (1984-1988 and 1993-1997) of the NMC data (update of Kodera (1995)).

3.3.1 Northern Winter

We start with the description of Fig. 5 for the northern hemispheric winter, which is better represented in the models than the southern hemispheric winter. In the observations a positive wind anomaly at the subtropical stratopause region in November/December propagates poleward and downward with time until January, then a negative anomaly appears which is further established in February (Kodera, 1991). This time evolution of mean zonal mean wind anomalies is very similar to the polar night jet oscillation (PJO) described in Kuroda and Kodera (2001). New studies (Kuroda and Kodera, 2002) suggest that the time evolution of the PJO is triggered by solar forcing in early winter.

Concentrating first on such models that used the GISS ozone (GISS and MRI-G), one can clearly see the poleward and downward propagation of the positive wind anomaly in the GISS model which is comparable to observations, but slightly too fast (refer, for example to January) and smaller in magnitude, except for

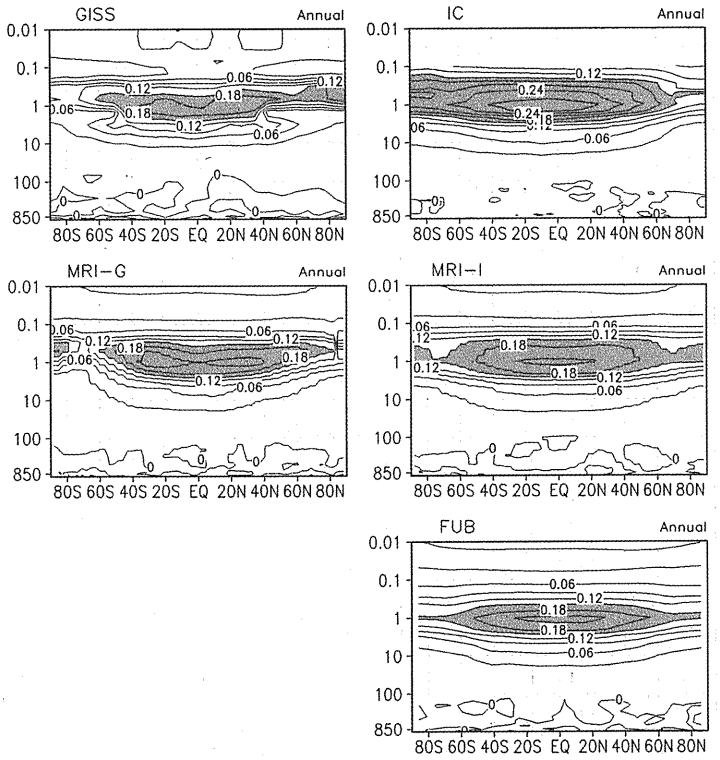

Fig. 3: Annual mean shortwave heating rate differences between the 20-year mean of the solar maximum experiment and the 20-year mean of the solar minimum experiment in Kelvin per day, contour interval: 0.03 K/d; values greater than 0.15 K/d shaded for emphasis. Left-hand column: GCMs using the GISS percentage ozone changes; right-hand column: GCMs using the IC percentage ozone changes.

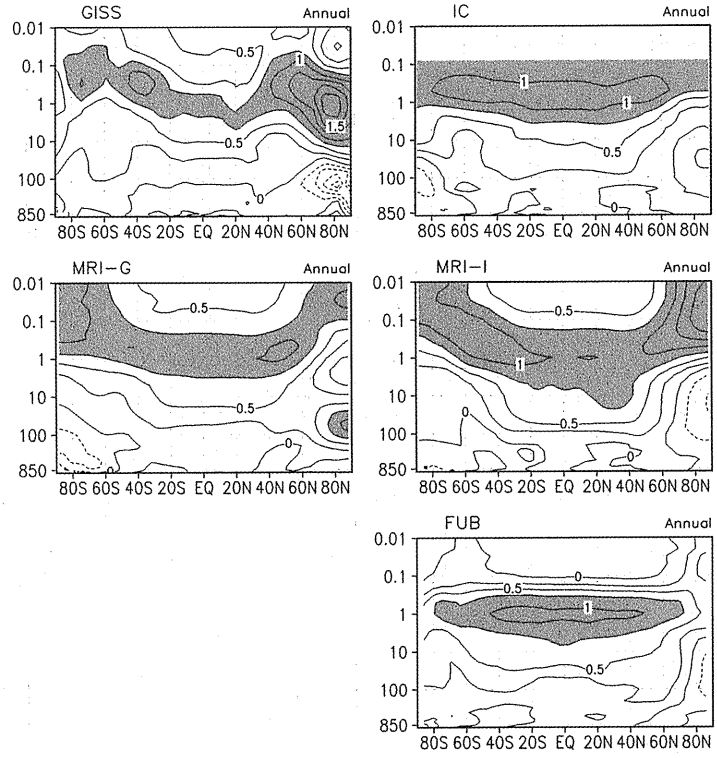

Fig. 4: Same as Fig. 3 but for the annual mean temperature differences in Kelvin, contour interval: 0.25 K, values greater than 0.75 K shaded for emphasis.

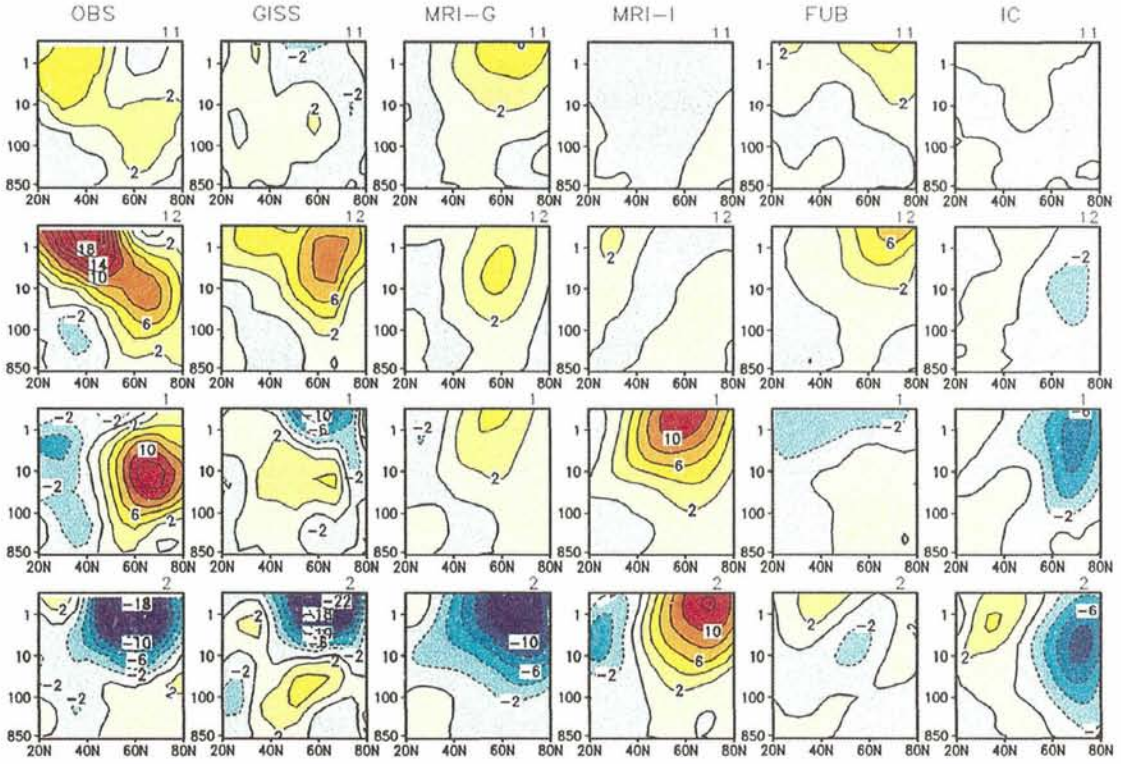

Fig. 5: Mean zonal mean wind differences between the 20-year mean of the solar maximum experiment and the 20-year mean of the solar minimum experiment in metres per second for the NH (20°-80°N) winter (November to February, top to bottom), contour interval 2 m/s. From left to right: observations (NMC data from 1980-1997; update of Kodera (1995)), GISS model, MRI-G experiment, MRI-I experiment, FUB model, and IC model.

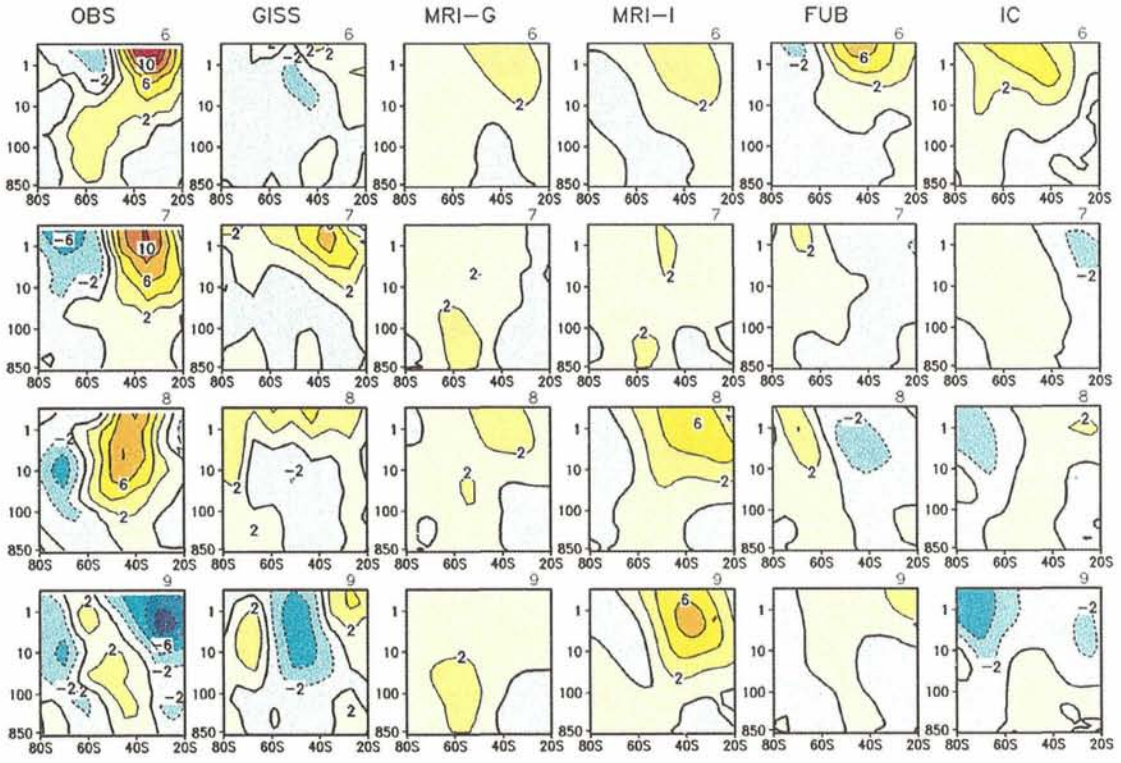

Fig. 6: Same as Fig. 5 but for the SH winter (June to September, top to bottom).

February where the negative anomalies reach -22 m/s, similar to observations (-18 m/s). The MRI-G experiment shows from November to January a positive wind anomaly of 4-6 m/s at higher stratospheric latitudes, which means a stronger polar night jet during solar maxima, but the magnitude of the mid-winter westerly anomalies is too small compared with observations. There is no apparent downward or poleward propagation and in February the model "switches" suddenly to a weaker polar night jet (negative anomaly), which is featured in the observations, but is extended too far down into the troposphere in the model.

Now the experiments that used the IC ozone changes are studied revealing differences and similarities compared to the above described model experiments. The MRI-I experiment showed a weak dipole structure in December with positive wind anomalies in the subtropical stratopause region and a negative anomaly at higher latitudes, this December structure is comparable to the November structure in the NMC data and GISS model results. In January a strong positive wind anomaly (10 m/s) was seen throughout higher stratospheric latitudes and weak negative anomalies were found at lower latitudes similar to observations. In February this dipole structure was further established but in contrast to observations no negative anomaly appeared at high latitudes (no weakening of the polar night jet). The evolution in the MRI-I experiments seemed to be delayed compared to observations (e.g., February of MRI-I similar to January in NMC).

Remarkable was the difference between the MRI-G and MRI-I experiment: the MRI-G experiment showed the same picture from November to January with weak westerly anomalies north of 40° N and weak easterlies equatorward and did not feature the westerly anomaly in the subtropical stratopause region, as observed and indicated in December in the MRI-I experiment. January was quite similar in both experiments but the magnitude of the westerly anomalies was smaller for the MRI-G experiment. In February, however, the wind signal for the two ozone fields was totally different. While the MRI model with GISS ozone produced easterly anomalies at high northern latitudes comparable to observations, the MRI model with IC ozone produced the reversed signal with westerly anomalies of approximately the same magnitude (+/- 12 m/s). This behaviour can be partly attributed to the used ozone field (IC or GISS) because this was the only difference between the two experiments and will be discussed in more detail in the next section.

Another aspect is the large interannual variability at high latitudes during winter which could be different for the MRI-I and the MRI-G experiment. The FUB model featured a positive wind anomaly (4 m/s) as early as November in the upper and middle stratosphere with two maxima, one around 30° N - similar to observations - and another at around 70° N - similar to the MRI-G experiment. In December the high latitude westerly anomaly (6 m/s) was further established and comparable to the MRI-G experiment from November to January. In January negative anomalies appeared around the stratopause and the structure was very similar to observations, except that the magnitudes were too small. In February, weak easterly anomalies (-2 m/s) appeared in the middle stratosphere and a westerly anomaly (+2 m/s) around 30° N, 1 hPa. The response of the FUB model was rather weak and the poleward and downward movement was hard to determine, which was also the case for the MRI and the IC model. This may be a problem of using monthly mean data which tend to smooth smaller maxima and minima in the anomalies. The IC model response was different again, except for November where it resembled the FUB model, although both models produced here an opposite response north of 60° N compared to observations. Through the winter the IC model showed a steady weakening of the polar night jet during solar maxima. In February a positive wind anomaly appeared around the subtropical stratopause region as can be seen in observations already in early winter; the structure of the anomalies in this month is similar to the one for the MRI-G experiment.

The MRI-I experiment was the only one that produced strong westerly anomalies throughout the stratosphere in February; all other models as well as the observations showed easterly anomalies. In the lower stratosphere and upper troposphere westerly anomalies appeared at middle and high latitudes in observations, which were reproduced in the GISS model and the MRI-I experiment. The MRI-G experiment, the FUB model and the IC experiment, on the other hand, displayed easterly anomalies in this region.

3.3.2 Southern Winter

To see how the models perform in the Southern Hemisphere (SH) the monthly zonal mean wind differences between solar maximum and minimum similar to Fig. 5 are shown in Fig. 6 for the southern hemispheric winter (from June to September). In the observations (first column) the anomalies in June in the SH were comparable with the November anomalies for the NH. In the subtropical stratopause region a

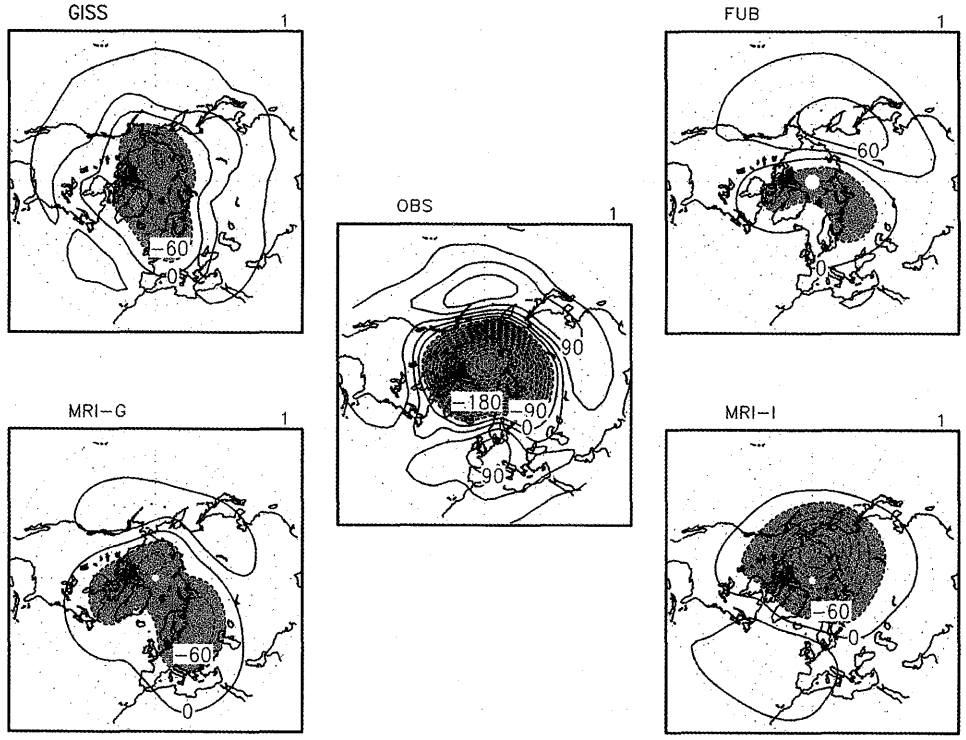

Fig. 7: Difference in the geopotential height at 30 hPa (~24 km) between the 20-year mean of the solar maximum experiment and the 20-year mean of the solar minimum experiment in geopotential meters (gpm), Contour interval 30 gpm, values less than -30 gpm shaded for emphasis; for northern winter (January) from 20°-90° N. Left-hand side: GCMs that used the GISS ozone, middle: observations (NMC data), right-hand side: GCMs that used IC ozone.

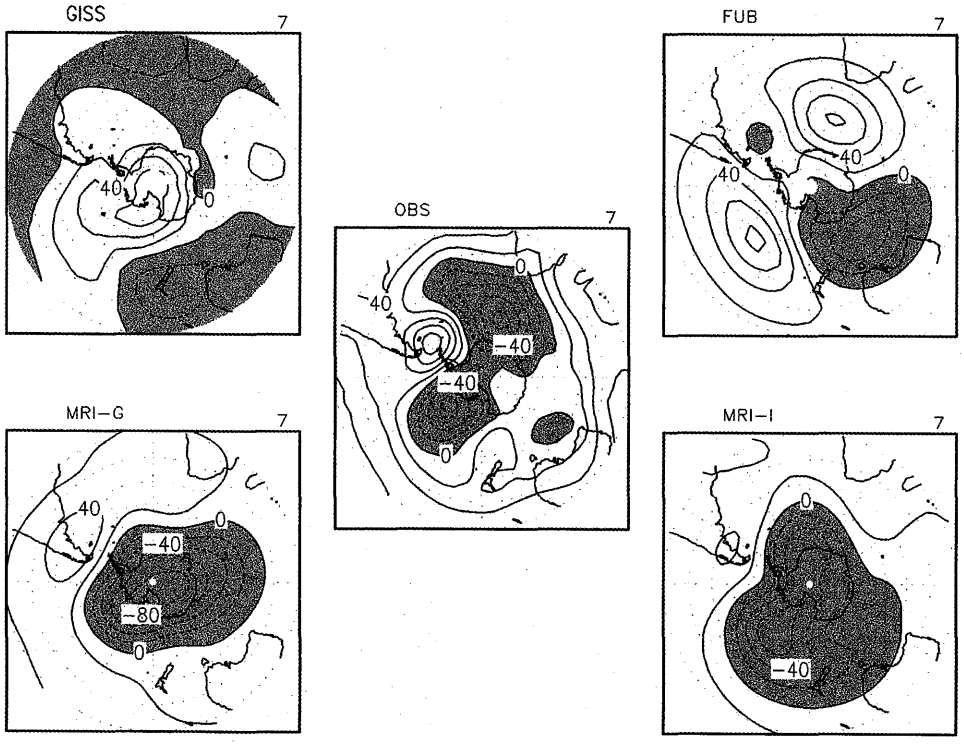

Fig. 8: Same as Fig. 7 but for the southern hemispheric winter (July) 20°-90° S, contour interval 20 gpm, negative values shaded for emphasis.

westerly wind anomaly appeared and a secondary one near 60° S in the lower stratosphere and upper troposphere. At higher latitudes easterly wind anomalies were apparent around the stratopause region. In contrast to the NH the positive wind anomaly propagated very slowly poleward and downward with time. A dipole structure with positive anomalies at lower latitudes and negative anomalies at higher latitudes persisted from June to August, reaching down into the lower stratosphere and upper troposphere. In September a stratospheric tripole structure can be seen with easterly anomalies at high and low latitudes and a westerly anomaly in between. The slower poleward and downward propagation for the SH has already been shown in Kuroda and Kodera (2001).

In all models a weak, westerly anomaly appeared in June in the subtropical stratopause region. The observed dipole structure near the stratopause can be seen in the MRI-I experiment and the FUB model; the magnitude was stronger for the FUB model. This weak model structure disappeared with time, leading to completely reversed results compared with observations, e.g., in the GISS model for late winter (September). The MRI-I experiment showed a very pronounced dipole structure in August and September with westerly anomalies of 6 m/s slightly weaker than the structure in June/July in the NMC data.

3.4 Geopotential Height

To show not only the zonal mean responses of observations and models but also the spatial patterns, stereographic projections for the geopotential height differences between solar maximum and solar minimum in the lower stratosphere (at 30 hPa) for the northern winter (January) are presented in Fig. 7. In Fig. 8 those same responses are shown for the southern winter (July). Remembering that the strongest response in the wind anomalies appeared for nearly all models in January for the NH the geopotential height differences for this month are plotted here. Observations are shown in the middle of the Figure, models with GISS ozone on the left-hand side and models with the IC ozone on the right-hand side. The 3-D data from the IC model is not available at present.

3.4.1 Northern Winter

In the observations a stronger polar vortex (negative geopotential height anomalies of -420 gpm) during solar maxima and higher geopotential heights at lower latitudes with two maxima in the area of the Aleutian high (+120 gpm) and over Europe (+90 gpm) can be seen. A generally similar structure with lower geopotential heights at high latitudes and higher geopotential heights at lower latitudes appeared in

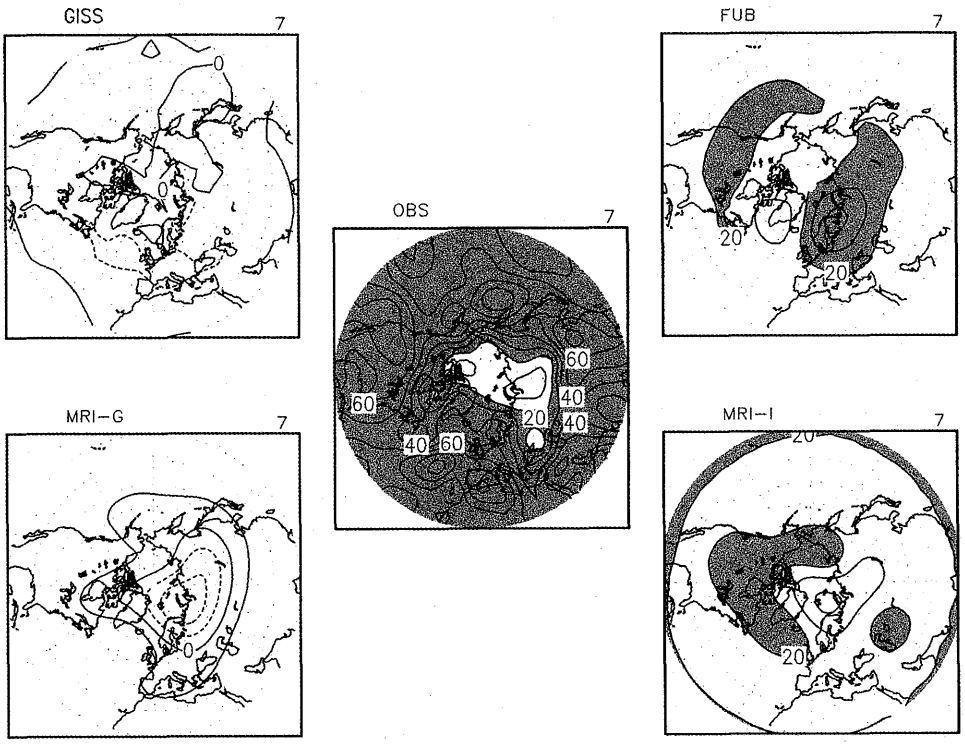

Fig. 9: Same as Fig. 7 but for the northern summer (July), contour interval 10 gpm, values larger than +20 gpm shaded for emphasis.

every model experiment although details differed from model to model and the magnitude of the anomalies was much weaker than in observations. The GISS and FUB models as well as the MRI-G experiment showed an elongated polar vortex at a position nearly corresponding to that observed (GISS: -120 gpm, FUB: -60 gpm, MRI-G: -60 gpm) with higher geopotential heights surrounding the negative anomalies concentrated over the Pacific Ocean (GISS: +30 gpm, FUB: +60 gpm, MRI-G: +30 gpm). The MRI-I experiment produced much stronger differences in the polar vortex (-210 gpm) than the MRI-G experiment. The maximum of positive geopotential height anomalies (+30 gpm) for the MRI-I experiment can be found over the Atlantic whereas it was located over the Pacific for all other model experiments.

3.4.2 Southern Winter

The strongest response in the mean zonal mean wind anomalies for the SH appeared in July (see Fig. 6), therefore geopotential height anomalies at 30 hPa are shown for this month in Fig. 8. The observations (middle) showed a large wave number 2 pattern with two negative anomalies south of Africa (-80 gpm) and over the Pacific side of Antarctica (-60 gpm), two positive anomalies between South America and Antarctica (+80 gpm) and a weaker one between Antarctica and Australia. Only the FUB model reproduced the observed wave number 2 pattern with a realistic amplitude but a phase shift of 90 degrees compared to the observations. All other models showed a pronounced wave number 1 pattern. The two models using the GISS ozone produced a totally reversed picture with a negative anomaly over Antarctica (-80 gpm) in the MRI-G experiment and a positive anomaly (+60 gpm) in the GISS model. Unlike the zonal mean wind case, the MRI-I and MRI-G experiment showed a very similar response with negative anomalies over Antarctica, surrounded by positive anomalies.

3.4.3 Northern Summer

The largest solar signal in observations can be found in northern summer (e.g., van Loon and Labitzke, 2000) for the lower stratosphere, therefore we focus now on the simulation of northern summer in the models. July was chosen as a characteristic northern summer month (Fig. 9) and the 30 hPa level as representative for the lower stratosphere. The observations revealed a belt of higher geopotential heights during solar maxima around 50° N of 60-80 gpm. In the northern polar region the anomalies were still positive but smaller in magnitude (~10-30 gpm). None of the models was able to reproduce the magnitude of the observed geopotential height differences.

The GISS model and the MRI-G experiment even showed the opposite (negative response) in the polar region, whereas the FUB model and the MRI-I experiment showed weak positive anomalies (10-20 gpm). In the MRI-I experiment and the FUB model an indication of a belt of higher geopotential heights around 40-50° N can be found which was more pronounced for the FUB model. However, the magnitude of the modelled height anomalies was only one third of that observed. In particular, the higher geopotential heights at lower latitudes were underestimated by the models.

4. Discussion

The equatorial temperatures in the middle atmosphere (Fig. 4) show the most consistent response to the increased shortwave heating rate (Fig. 3) due to enhanced solar UV irradiance and ozone. In some of the model experiments (MRI, FUB, UIUC) presented only spectral solar irradiance changes in the UV part of the solar spectrum (200-420 nm) were taken into account which led to a warming near the stratopause during solar maximum through stronger absorption of UV light and altered ozone production and loss in the stratosphere. The 11-year change in absorption in the visible part of the spectrum (Chappuis band 400-800 nm) by ozone was neglected in these model studies as was the change in absorption due to the visible irradiances changes at the Earth's surface which is mostly covered with water. The GISS and the IC model did include the visible and near-infrared changes of solar irradiance variations, but the effect of the surface warming through absorption of visible light of 11-year periodicity should be considerably attenuated by the large heat capacity of the ocean. Therefore all model studies presented here used seasonally varying climatological SSTs. However, atmospheric dynamical changes can drive oceanic circulation changes (and vice versa, e.g. ENSO). So for a proper simulation of the Hadley cell over the 11-year solar cycle and of processes in the lower stratosphere, a coupled ocean-middle atmosphere model should be used, which is however presently very expensive to run.

The temperature signal at higher latitudes varied from model to model. Similarly, it was very difficult to find a systematic model signal in the zonal-mean zonal wind in the NH. Each model response was different even though the inputs were similar: the signal seemed to be only dependent on the ozone change field and on the model dynamics. The GISS model alone produced some downward and poleward propagation similar to observations. None of the models were able to properly

capture the strong westerly anomalies in the subtropical stratopause region in December, although a weak indication of such an anomaly was evident in the FUB model in November and in the GISS and the MRI-I models in December.

The response in the zonal-mean zonal wind in the SH was too weak and mostly not comparable with observations. Interestingly, the GISS model, which produced fairly good results for the NH performed less well in the SH. The MRI-I experiment on the other hand reproduces some of the westerly anomaly patterns seen in the observations, albeit shifted in time. Each GCM had its own problems in simulating the response in both hemispheres, compared to observations so it was very difficult to nominate a "best" model for simulating the signal in both hemispheres.

A generally similar structure with lower geopotential heights at high latitudes and higher geopotential heights at lower latitudes appeared in every model experiment although details differed from model to model and the magnitude of the anomalies was much weaker than in observations in NH winter (Fig. 7). One has to take care in comparing the 30 hPa height level in observations directly with the same height level in the models because often a stronger response in the models appears higher up due to differences of observed and modelled climatologies. This phenomenon is apparent for the January wind differences in Fig. 5: the maximum of the westerly wind anomaly observations occurred around 10 hPa, similar to the GISS and the FUB models, but more than three orders of magnitude larger than in the models. For the MRI experiments it occurred much higher around 1 hPa. Additionally, for the GISS model, the largest responses occurred in December and February, then the model is much closer to observations. The above findings suggest to concentrate mostly on the principle patterns, not on the magnitude of the simulated responses.

The magnitude of the observed geopotential height differences for the SH was much smaller than that for the NH which could be due to the smaller variability in the SH. The difference in the hemispheric variability was reproduced in all models. The discrepancy between modelled and observed geopotential height anomalies may be partly accounted for by the missing QBO in the models. The QBO is not spontaneously produced nor forced in the GCMs. In their basic state, all GCMs produce weak easterly winds in the equatorial lower stratosphere. In the real atmosphere, the variability at equatorial latitudes is produced by the QBO which may also influence higher latitudes. Salby and Callaghan (2000) and Soukharev and Hood (2001) found an 11-year solar cycle in the QBO data itself and other authors have found a modulation between the solar and the QBO signal (e.g. Labitzke and van Loon, 1987; Kodera and Kuroda, 2002). Recently, Gray et al. (2001a,b) showed the importance of tropical upper stratospheric winds and their effect on the polar lower stratospheric region. But so far no evidence for the influence of the QBO in this way has been found and further model studies are needed to shed more light on this problem.

4.1 Model Climatology

Up to now, we have focused on the difference of the model response between the solar maximum and minimum experiments. This would be sufficient if the response varied linearly with the forcing. However, the change of the solar forcing generates non-linear dynamical effects in the winter stratosphere. Thus, we also need to investigate the difference in the climatology among the models and not only the response to the changed forcing.

Figure 10 shows the NH zonal mean wind climatology for the solar maximum case and the standard deviation. For the discussion a fifth GCM experiment with interactively calculated chemistry from the University of Illinois (UIUC) is also shown. This GCM performed two 15 year solar experiments using the same spectral irradiance data from Lean et al. (1997) and calculated the ozone differences between solar maxima and minima directly through changes in the shortwave radiation and changes in the photolysis rates. The solar maximum case was chosen because new studies (Kodera and Kuroda, 2002) have found a significantly stronger signal in early winter due to the longer lasting radiatively controlled state during this phase of the solar cycle compared to the solar minimum case.

The observed double peaks in the standard deviation around the stratopause in December, which correspond to the subtropical jet around 30° N and the polar night jet around 60° N as defined in Kodera and Kuroda (2002), were not evident in the GCMs. In most GCMs the standard deviation at high latitudes was already strong in early winter, e.g., in the FUB, the MRI-I and the UIUC models. In the case of the FUB model this is probably due to its large internal year-to-year variability which starts earlier than observed (not explicitly shown here). None of the GCMs shows a polar night jet similar to observations - this is a well-known phenomenon, the polar night jet in GCMs is confined to high latitudes and fails to tilt equatorward. The strong jet leads to the so-called "cold-bias" problem in the lower stratosphere at high latitudes. A

parameterisation of orographic and non-orographic gravity waves is one probable solution to achieve a polar night jet similar to observations (e.g., McLandress, 1998). Sometimes, the gravity wave parameterisation suppresses all variability. Then a very weak polar night jet and a "warm-bias" are the result, which may be even more problematic than a "cold-bias". Often the coarse horizontal and vertical resolution in GCMs is not sufficient to resolve small-scale structures like gravity waves. The GCMs presented here employ differing GW parameterisations (see Table 1). Another important aspect for the discrepancy between the observed and modelled climatologies could be the missing QBO which produce a fairly high variability throughout the equatorial stratosphere (e.g., Gray et al., 2001a,b).

The GISS model is the only one showing a larger standard deviation in the subtropical stratopause region in December and a secondary peak at 65° N. This can also be seen in the mean zonal mean wind differences in Fig. 5. The GISS model is the only one showing pronounced westerly anomalies in the subtropical stratopause region in December. In the MRI-I model weak westerly anomalies can also be seen in this month. All other models show a larger standard deviation in the polar stratopause region, which is rather small for the IC and the UIUC models. The magnitude of the polar night jet (70 m/s) in December in the NMC data is weaker than the GISS model (90 m/s). The FUB model (100 m/s), and the IC model (80 m/s) are stronger than the MRI-G (60 m/s) and MRI-I (60 m/s) experiments, and much stronger than the UIUC model (50 m/s). In January and February nearly all model winds are 10-30 m/s stronger than the observed winds. The difference in the wind climatology for the MRI experiments that we have already shown in Fig. 5 for the mean zonal mean wind differences is interesting. The only difference between these two experiments was the 2-D-ozone change field. While in the model experiment with the IC ozone the MRI model tends to enhance the wind, it tends to lower it using the GISS ozone. This behaviour can be clearly seen for February where the MRI-I experiment was the only one showing a stronger polar night jet during solar maximum compared to all other models (see Fig. 5).

Another interesting point is the fact that a few models

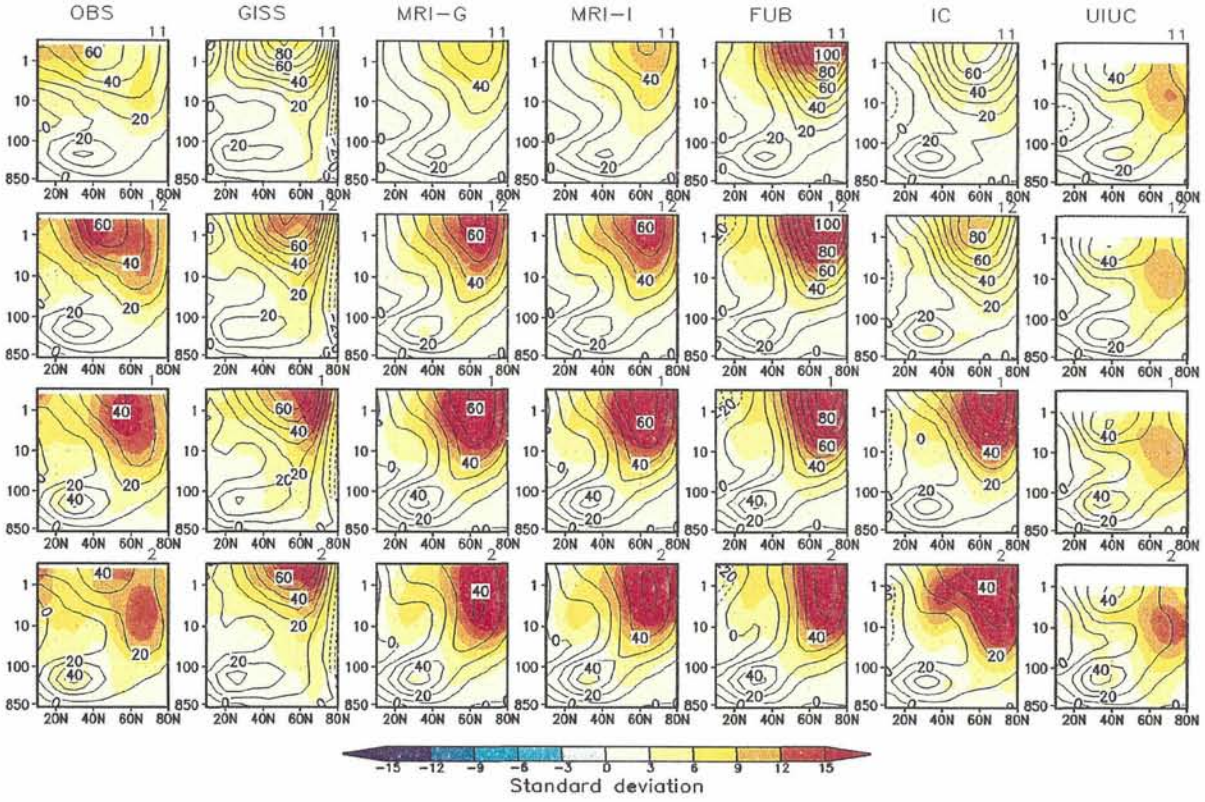

Fig. 10: Mean zonal mean wind climatology for the solar maximum cases (contour interval 10 m/s) and standard deviation (shading interval 3 m/s) for the NH (20°-80° N) from November to February (top to bottom); from left to right: Observations (6 years of NMC data), GISS model, MRI-G experiment, MRI-I experiment, FUB, IC model, UIUC model (for each of the model experiments a 20-year climatology is shown, except for the UIUC model, here only 15 years are included).

showed a secondary peak in the standard deviation around the subtropical stratopause not in early winter (December) as in observations, but a little bit later. In the IC model this can be clearly seen in February and corresponds well with the westerly wind anomaly in this region as seen in the zonal mean wind differences in Fig. 5. In the UIUC model, the standard deviation is very small in the upper stratosphere, particularly, in the subtropics throughout the winter. This apparently reflects the low model top at 1 hPa, which dampens planetary waves propagating up into the equatorial stratopause region.

4.2 Observed variations in ozone and temperature

The present study focused mainly on the differences among the model simulations. One of the peculiarities of the solar influence is that there is no firm observational evidence. Observational results have their own problems due to the shortness of the homogeneous data sets or due to instrumental calibrations. It is also difficult to distinguish the solar signal from other sources of variability.

There are different types of instruments measuring ozone as well as temperature: 1) ground-based instruments (radiosonde, rocket sonde, and lidar), and 2) satellite instruments (microwave, UV and infrared sounders). The post-processing of satellite data has to take into account problems due to temporal discontinuity, instrument calibration (area and weight factor), and orbit drift. Especially, overlapping periods of different satellite instruments can cause problems if the respective time series have to be fitted together (e.g., Frohlich, 2000). There are further natural disturbances, such as volcanic eruptions, which can lead to an increase in the stratospheric aerosol amount for 1-2 years following the eruption and influence the chemical and radiation budget of the atmosphere. Volcanic aerosol also directly disturbs the satellite measurements. Often years following large volcanic eruptions (Mount Agung, 1963; El Chichon, 1982; Mount Pinatubo, 1991) are neglected in data sets to eliminate these effects. Volcanic aerosols (sulfate aerosols) provide a catalyst for stratospheric ozone depletion and counteracted the ozone increase during solar maximum years in which a volcanic eruption took place, i.e. in 1982 and 1991.

The same problem of data reliability exists for temperature measurements. Satellite based measurements are only available since 1979 and usually have quite a coarse vertical resolution. There is no data set covering the whole atmosphere from the troposphere up to the mesosphere. Observed temperature signals have to be viewed with caution because they depend on the source of the data (instrument specialities such as the vertical resolution etc.), the time interval of measurements, and the method with which the temperature signal was extracted from the raw data (Ramaswamy et al., 2001). Often a statistical multiple linear regression model is used to extract the solar signal. These statistical models usually take into account a linear trend term, a QBO term, an ENSO term, a solar forcing term, and an aerosol term (for the volcanic signal) and are able to extract with this method each of the assumed natural or anthropogenic contributions. If a volcanic signal (warming of the lower stratosphere) coincides with a warming due to the maximum phase of the solar cycle as happened in 1982 and 1991, it is important to separate the volcanic and the solar signal in temperature time series (e.g., McCormack et al., 1997).

The solar signal in temperature extracted from different data sets shows discrepancies. For example, McCormack and Hood (1996), analysed NMC data from 1980 to the year 1995, and found positive annual mean temperature signals due to the 11-year solar cycle of 2-2.5 K (from 30° S to 30° N near the stratopause (their Fig. 4)); of 1.5 K (from 40°-60° north and south around 37 km height), and even negative temperature anomalies in the equatorial middle stratosphere around 32 km height. In contrast, the strongest temperature signal in the WMO report (1999), estimated with a regression model from SSU and MSU data, suggested 0.75 K in the equatorial upper stratosphere at around 40 km height which decayed further up and even reached negative anomalies above 50 km.

All GCM experiments presented here produced a large temperature signal of 0.75-1 K around the stratopause (see Fig. 4). None of the GCMs showed a negative temperature signal in the middle stratosphere as found in McCormack and Hood (1996). A similar positive temperature signal was also found in the UIUC GCM. The annual mean temperature differences between 15 solar maximum and 15 solar minimum years for this model are shown in Fig. 11. They can be directly compared with Fig. 4. Although the top of this GCM is close to the stratopause, it showed a quite similar temperature response to the other GCMs, featuring higher temperatures of 0.75-1 K around 1 hPa. These results suggest that the interactively calculated ozone does not give a qualitatively different or better response than the GCM experiments using specified ozone. The impact of interactively calculated ozone should be further studied with other GCMs extending into the mesosphere.

4.3 Uncertainty of calculated ozone and solar variability

The discrepancy between model simulations and observations also arises from an uncertainty of the solar forcing and calculated ozone variations which were used as input for all model experiments. First of all, reliable observed solar UV variations are limited in that they are only available for a relatively short time starting from 1979, with the advent of satellite-borne radiometers. This is the reason why the interest for sun-climate interactions has increased in recent years, and why model studies with realistic wavelength-dependent irradiance changes have become possible. Many processes associated with the sun itself are not yet fully understood. The mechanisms for the irradiance variations are still not properly known and the long-term trend in total solar irradiance and especially the difference in the current solar cycle (solar cycle 23) compared to earlier cycles needs to be studied in more detail (e.g. Pap, 2001).

As already mentioned above, solar UV irradiance variations alter the ozone loss and production in the stratosphere. During solar maximum enhanced solar UV radiation enhances the photochemical production of ozone in sunlit areas of the stratosphere - the efficiency of this process depends on the ozone amount in different stratospheric layers, the different penetration/absorption of the UV radiation of different wavelengths, and the air density and temperature. The overall process is very complex and leads to the maximum ozone difference in percent between solar maximum and minimum appearing at around 5 hPa. This occurs despite the fact that the maximum shortwave heating rate difference can be found in the upper stratosphere near the stratopause (~50 km) and the maximum ozone amount can be found in the lower stratosphere (between 22-24 km). Resulting uncertainties in the vertical distribution of ozone changes due to the 11-year solar cycle especially in the region of the tropopause, and in the middle and upper stratosphere (compare, e.g., Fig. 2a and 2b) have an impact upon temperature changes in these altitudes regions.

Usually 2-D models reproduce a maximum of ozone variability with the 11-year solar cycle on the order of 2-3% around 5 hPa, whereas the observations suggest 5% of solar cycle variation at 1 hPa (e.g., Brasseur, 1993, Hood et al., 1993, McCormack and Hood, 1996, McCormack et al., 1997). This under-estimation may be due to the missing dynamic feedback in 2-D models (although some use parameterised effects of gravity waves and planetary waves). It could also be due to the lack of interactively calculated ozone, an overestimated ozone signal from observations, or due to an incomplete understanding of ozone chemistry. An interactive calculation of ozone in UIUC model did not lead to an improvement of the simulation. The ozone variation in the low top UIUC model is not so different from that in the IC 2-D model. However, the insufficiency of wave mean-flow interaction in the subtropics of the upper stratosphere, which manifests itself in a small interannual variability of the zonal wind, leads to the fact that the mean meridional circulation cannot be adequately simulated in this model. This suggests that for a correct representation of the circulation and especially the mean meridional circulation, a mesosphere has to be included.

A non-negligible effect of NOy flux changes during the 11-year solar cycle has been suggested to be important (e.g., Callis et al., 2000) and should be taken into account in model studies. During solar minimum years the NO_y flux from the mesosphere is stronger and the formed NO_2 is transported into the stratosphere where it leads to an additional ozone destruction. If this effect is not taken into account the simulated ozone difference between solar maximum and minimum could be underestimated. Further modelling studies are needed to solve this problem and longer data sets are needed to obtain more statistically reliable data.

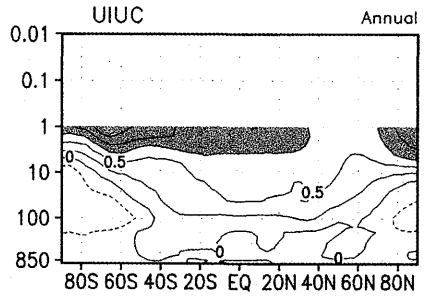

Fig. 11: Same as Fig. 4 but for the University of Illinois GCM with fully interactive chemistry.

5. Concluding Remarks

As has been suggested in the discussion, one important pre-requisite in trying to simulate the 11-year solar signal with GCMs could be a realistic model climatology. Further work is needed to improve the models' climatology, which have an impact on the wave propagation properties, the wave-mean flow interaction and on the representation of the mean meridional circulation which has been shown to be modulated by the solar cycle (Kodera and Kuroda, 2002). As long as the climatology is not properly represented in GCMs we cannot expect solar simulations to be comparable to observations. A factor which further complicates the

solar signal is the QBO.

The GISS model appeared to show a zonal mean response most like the observations in the NH even though its wind climatology was not better than the other GCMs (except for December where it was the only GCM showing a higher standard deviation in the subtropical stratopause region). This could be one reason for its relatively good correspondence with observations. It was however difficult to select a "best" model for representing both hemispheres adequately. It turned out that the GCMs were sensitive to the ozone change field which can be clearly seen, not only by comparing the different GCMs that used the two ozone change fields, but also by comparing the simulations using the two ozone change fields in the same GCM.

From all points discussed one could speculate that the "unrealistic" dynamics in the models lead to a temperature signal that is mainly radiatively controlled in early winter. In later winter the signal is a combination of radiative effects in the models (dependent on the radiation schemes) and internal model dynamics, which is not comparable to observations. Improving the model climatologies and therefore the dynamics could maybe lead to a temperature signal that is more comparable with observations. In summary, to achieve a better understanding and for better defining future comparison studies, the model climatologies need to be improved and the ozone difference between solar maximum and minimum need to be further studied with chemistry models. Also, the derivations of observed solar signals in temperature and ozone need to be improved.

6. Acknowledgements

We would like to thank J. Lean for providing the wavelength-dependent solar irradiance data and S. Pawson for the coordination of the GRIPS project. This work is supported in part by a Bilateral International Joint Research Program of the Japanese Agency for Science and Technology, and resulted from two stays of the first author (Katja Matthes) at the Meteorological Research Institute (MRI) in Tsukuba, Japan. The study has also been partly funded by the European Commission under the contract No. EVK2-CT-1999-00001 (SOLICE). The integrations with the FUB-CMAM and further diagnostics were performed on the CRAY J932/16-8192 of the Konrad-Zuse-Zentrum fur Informationstechnik Berlin (ZIB).

7. References

Brasseur, G., 1993: The response of the middle atmosphere to long-term and short-term solar variability: A two-dimensional model. *J. Geophys. Res.*, 98, 23079-23090.

Briegleb, B. P., 1992: Delta-Eddington approximation for solar radiation in the NCAR community climate model. *J. Geophys. Res.*, 97, 7603-7612.

Callis, L. B., M. Natarajan, and J. D. Lambeth, 2000: Calculated upper stratospheric effects of solar UV flux and NOy variations during the 11-year solar cycle. *Geophys. Res. Lett.*, 27, 3869-3872.

Chou, M. D., 1990: Parameterizations for the absorption of solar radiation by O_2 and CO_2 with application to climate studies, *J. Clim.*, 3, 209-217.

Chou, M. D., 1992: A solar radiation model for use in climate studies, *J. Atmos. Sci.*, 49, 762-772.

Chou, M. D., and K. T. Lee, 1996: Parameterization for the absorption of solar radiation by water vapor and ozone, *J. Atmos. Sci.*, 53, 1203-1208.

Chou, M.D., and M. J. Suarez, 1999: A solar radiation parameterization for atmospheric studies, in Technical Report Series on Global Modeling and Data Assimilation, v.15, 40 pp., NASA Greenbelt, Md.

Edwards, J.M., and A. Slingo, 1996: Studies with a flexible new radiation code. I: Choosing a configuration for a large-scale model, *Q. J. R. Meteorol. Soc.*, 122, 689-719.

Fortuin, J.P.F., and U. Langematz, 1994: An update on the global ozone climatology and on concurrent ozone and temperature trends, SPIE Atmospheric Sensing and Modeling, 2311.

Fouquart, Y., and B. Bonnel, 1980: Computations of solar heating of the Earth's atmosphere: a new parameterization, Beitr. Phys. Atmos., 52, 1-16.

Fröhlich, C., 2000: Observations of Irradiance Measurements. *Space Sci. Rev.*, 94, 15-24.

Gray, L. J., E. F. Drysdale, T. J. Dunkerton, and B. N. Lawrence, 2001a: Model studies of the interannual variability of the Northern Hemisphere stratospheric winter circulation: the role of the Quasi Biennial Oscillation. *Q. J. R. Meteorol. Soc.*, 127, 1413-1432.

Gray, L. J., S. J. Phipps, T. J. Dunkerton, M. P. Baldwin, E. F. Drysdale, and M. R. Allen, 2001b: A data study of the influence of the equatorial upper stratosphere on Northern Hemisphere stratospheric sudden warmings. *Q. J. R. Meteorol.* Soc., 127, 1985-2003.

Haigh, J. D., 1994: The role of stratospheric ozone in modulating the solar radiative forcing of climate. *Nature*, 370, 544-546.

Haigh, J. D., 1996: The impact of solar variability on climate. *Science*, 272, 981-984.

Haigh, J. D., 1999: A GCM study of climate change in

response to the 11-Year solar cycle. *Q. J. R. Meteorol. Soc.*, 125, 871-892.

Hansen, J., G. Russell, D. Rind, P. Stone, A. Lacis, S. Lebedeff, R. Ruedy, and L. Travis, 1983: Efficient three-dimensional global models for climate studies: Models I and II. *Mon. Weather Rev.*, 111, 609-662.

Keating, G.M., D.F. Young, and M.C. Pitts, 1987: Ozone reference models for CIRA, *Adv. Space Res.*, 7, 105-115.

Kodera, K., 1991: The solar and equatorial QBO Influences on the stratospheric circulation during early northern winter. *Geophys. Res. Lett.*, 18, 1023-1026.

Kodera, K., 1995: On the origin and nature of the interannual variability of the winter stratospheric circulation in the northern hemisphere. *J. Geophys. Res.*, 100, 14077-14087.

Kodera, K., and Y. Kuroda, 2002: Dynamical response to the solar cycle. *J. Geophys. Res.*, 107, 4749, doi:10.1029/2002JD002224.

Kodera, K., K. Matthes, K. Shibata, U. Langematz, and Y. Kuroda, 2003 : Solar impact on the lower mesospheric subtropical jet: a comparative study with general circulation model simulations, *Geophys. Res. Lett.*, 30(4), 1175, doi:10.1029/2002GL016584.

Kuroda, Y., and K. Kodera, 2001 : Variability of the polar-night jet in the northern and southern hemispheres. *J. Geophys. Res.*, 106, 20703-20713.

Kuroda, Y., and K. Kodera, 2002: Effect of the solar cycle on the Polar-Night Jet Oscillation. *J. Met. Soc. Japan*, 80, 973-984.

Labitzke, K., 1987: Sunspots, the QBO and the stratospheric temperature in the north polar region. *Geophys. Res. Lett.*, 14, 535-537.

Labitzke, K., 2001: The global signal of the 11-Year sunspot cycle in the stratosphere: Differences between solar maxima and minima. *Met. Zeitschrift*, 10, 901-908.

Labitzke, K., and H. v. Loon, 1988: Associations between the 11-year solar cycle, the QBO and the atmosphere, Part I: The troposphere and stratosphere in the Northern Hemisphere in Winter. *J. Atmos. Terr. Phys.*, 50, 197-206.

Labitzke, K. and H. v. Loon, 1999: The stratosphere: phenomena, history, and relevance. Springer Verlag, Berlin.

Langematz, U., 2000: An estimate of the impact of observed ozone losses on stratospheric temperatures. *Geophys. Res. Lett.*, 27, 2077-2080.

Langematz, U., and S. Pawson, 1997: The Berlin troposphere-stratosphere-mesosphere GCM: climatology and annual cycle. *Q. J. R. Meteorol. Soc.*, 123, 1075-1096.

Larkin, A., J. D. Haigh, and S. Djavidnia, 2000: The Effect of solar UV radiation variations on the Earth's atmosphere. *Space Sci. Rev.*, 94, 199-214.

Lean, J. L., G. J. Rottman, H. L. Kyle, T. N. Woods, J. R. Hickey, and L. C. Puga, 1997: detection and parameterisation of variations in solar mid- and near-ultraviolet radiation (200-400nm). *J. Geophys. Res.*, 102, 29939-29956.

McCormack, J. P., and L. L. Hood, 1996: Apparent solar cycle variations of upper stratospheric ozone and temperature: latitude and seasonal dependences. *J. Geophys. Res.*, 101, 20933-20944.

McCormack, J. P., L. L. Hood, R. Nagatani, A. J. Miller, W. G. Planet, and R. D. McPeters, 1997: Approximate separation of volcanic and 11-year signals in the SBUV-SBUV/2 total ozone record over the 1979-1995 period, *Geophys. Res. Lett.*, 24, 2729-2732.

McLandress, C., 1998: On the importance of gravity waves in the middle atmosphere and their parameterization in general circulation models. *J. Atmos. Sol.-Terr. Phys.*, 60, 1357-1383.

Pap, J. M., 2001: Total solar and spectral irradiance variations from near-UV to infrared, in: The variable shape of the Sun: Astrophysical Consequences. ed. J.P. Rozelot, Lecture Notes in Physics, Springer-Verlag, in press.

Pawson, S., U. Langematz, G. Radek, U. Schlese, and P. Strauch, 1998: The Berlin troposphere-stratosphere-mesosphere GCM: sensitivity to physical parameterizations. *Q. J. R. Meteorol. Soc.*, 124, 1343-1371.

Pawson, S., K. Kodera, K. Hamilton, T. G. Shepherd, S. R. Beagley, B. A. Boville, J. D. Farrara, T. D. A. Fairlie, A. Kitoh, W. A. Lahoz, U. Langematz, E. Manzini, D. H. Rind, A. A. Scaife, K. Shibata, P. Simon, R. Swinbank, L. Takacs, R. J. Wilson, J. A. Al-Saadi, M. Amode, M. Chiba, L. Coy, J. de Grandpre, R. S. Eckman, M. Fiorino, W. L. Grose, H. Koide, J. N. Koshyk, D. Li, J. Lerner, J. D. Mahlman, N. A. McFarlane, C. R. Mechoso, A. Molod, A. O'Neill, R. B. Pierce, W. J. Randel, R. B. Rood, F. Wu, 2000: The GCM-Reality Intercomparison Project for SPARC (GRIPS): Scientific Issues and Initial Results. *Bull. Am. Meteorol. Soc.*, 81, 781-796.

Ramaswamy, V., M. L. Chanin, J. Angell, J. Barnett, D. Gaffen, M. Gelman, P. Keckhut, Y. Koshelkov, K. Labitzke, J. J. R. Lin, A. O'Neil, J. Nash, W. Randel, R. Rood, M. Shiotani, R. Swinbank, and K. Shine, 2001: Stratospheric temperature trends: observations and model simulations. *Rev. Geophys.*, 39, 71-122.

Randel, W. J., 1992: Global atmospheric circulation statistics, 1000-1 mb, NCAR Tech. Note. NCAR/TN-366+STR, 256 pp., Nat. Cent. for Atmos. Res., Boulder, Colorado.

Rind, D., R. Suozzo, N. K. Balachandran, A. Lacis, and G. Russel, 1988a: The GISS global climate-middle atmosphere model, Part 1: Model structure and climatology. *J. Atmos. Sci.*, 45, 329-370.

Rind, D., R. Suozzo, and N. K. Balachandran, 1988b: The GISS Global Climate-Middle atmosphere model. Part 2: Model variability due to interactions between planetary waves, the mean circulations, and gravity wave drag. *J. Atmos. Sci.*, 45, 371-386.

Rozanov, E.V., Schlesinger, M.E., and Zubov, V.A., 2001: The University of Illinois, Urbana-Champaign three-dimensional stratosphere-troposphere general circulation model with interactive ozone photochemistry: Fifteen-year control run climatology. *J. Geophys. Res.*, 106 , 27233-27254.

Salby, M., and P. Callaghan, 2000: Connection between the solar cycle and the QBO: The Missing link. *J. Clim.*, 13, 2652-2662.

Shibata, K., and A. Uchiyama, 1994: An application of the discrete ordinate method to terrestrial radiation in climate models. *J. Atmos. Sci.*, 51, 3531-3538.

Shibata, K., H. Yoshimura, M. Ohizumi, M. Hosaka, and M. Sugi, 1999: A simulation of troposphere, stratosphere and mesosphere with an MRI/JMA 98 GCM. *Papers in Meteorol. and Geophys.*, 50, 15-53.

Shindell, D., D. Rind, N. Balachandran, J. Lean, and J. Lonergan, 1999: Solar cycle variability, ozone, and climate. *Science*, 284, 305-308.

Shindell, D. T., G. A. Schmidt, R. L. Miller, and D. Rind, 2001: Northern hemisphere winter climate response to greenhouse gas, ozone, solar, and volcanic forcing. *J. Geophys. Res.*, 106, 7193-7210.

Shine, K. P., and J. A. Rickaby, 1989: Solar radiative heating due to the absorption by ozone, Ozone in the Atmosphere, R. D. Bojkov and P. Fabian, Eds., Deepak, 597-600.

Soukharev, B. E., and L. Hood, 2001: Possible solar modulation of the equatorial Quasi-Biennial Oscillation: Additional statistical evidence. *J. Geophys. Res.*, 106, 14855-14868.

Strobel, D. F., 1978: Parameterisation of the atmospheric heating rate from 15 to 120 km due to O_2 and O_3 absorption of solar radiation, *J. Geophys. Res.*, 83, 6225-6230.

Swinbank, R., W. A. Lahoz, A. O'Neill, C. S. Douglas, A. Heaps, and D. Podd, 1998: Middle atmosphere variability in the UK Meteorological Office Unified Model. *Q. J. R. Meteorol. Soc.*, 124, 1485-1525.

van Loon, H., and K. Labitzke, 2000: The influence of the 11-year solar cycle on the stratosphere below 30 km: A review. *Space Sci. Revs.*, 94, 259-278.

Wang, W.-C., X.-Z. Liang, M.P. Dudek, D. Pollard, and S.L. Thompson, 1995: Atmospheric ozone as a climate gas. *Atmospheric Research*, 37, 247-256.

World Meteorological Organization, 1999: Scientific assessment of ozone depletion 1998. Global Ozone Res. and Monit. Proj., Rep. 44, Geneva.

GRIPS太陽影響モデル実験比較計画: 第1報

K. Matthes, K. Kodera, J. D. Haigh, D. T. Shindell, K. Shibata,
U. Langematz, E. Rozanov, and Y. Kuroda

GRIPS(中層大気大循環モデル国際比較計画)のうち11年太陽周期の大気に及ぼす影響に的を絞ったGRIPS参加各グループの大循環モデルによる数値実験の結果を示す。ここでは、将来のより詳細な太陽活動の影響の数値実験を行う上で、何が問題であるか明らかにすることを目的として比較を行う。それぞれの大循環モデル実験の結果がこれまでの実験や観測に比較して整合性のあるものかの吟味を行っている。より整合の取れた比較を行うために各大循環モデルには同一の、i)波長依存性をもつ太陽放射変化とii)それによって生じるオゾン変化を2次元光化学モデルで計算したものの双方を与えた。各モデル実験の比較の結果には明らかな違いが見られ、これはモデル間、あるいは観測との気候値の違いを反映していることが示唆される。この実験比較における大きな困難の一つは、モデル実験と比較する信頼できる気温やオゾンの太陽周期変化の影響の観測データが無い事による。また、モデルを駆動するのに与えた太陽エネルギー・スペクトラムやオゾンにもいまだ不確実性が残っている。